Iranian Journal of Catalysis 8(4), 2018, 297-309

IRANIAN JOURNAL OF CATALYSIS

Enhanced removal of methylene blue dye by bimetallic nano-sized MOF-5s

Mahshid Zebardast, Abdollah Fallah Shojaei*, Khalil Tabatabaeian

Department of Chemistry, University of Guilan, Rasht, P.O. Box: 4193833697, Iran.

Received 19 June 2018; received in revised form 16 September 2018; accepted 27 September 2018

ABSTRACT

Metal-organic framework 5 (MOF-5) and bimetallic MOF-5s (Co/Zn and Ni/Zn) were prepared via a simple solvothermal method. Samples were characterized by various techniques such as powder X-ray diffraction (XRD), Fourier transform infrared (FT-IR), scanning electron microscopy (SEM), UV-Vis diffuse reflectance spectroscopy (DRS), inductively coupled plasma (ICP) and elemental analysis (EA). Photocatalytic decolorization of methylene blue (MB) dye in the aqueous solutions was examined under UV and visible light irradiation. The degradation of MB solutions was calculated by changes in the UV–Vis absorbencies of the aqueous solutions at λ_{max} = 664 nm. The influence of various parameters such as the catalyst loading, dye concentration, initial pH of the dye solution and adding electron acceptors (H_2O_2, tert-Butyl hydroperoxide (TBHP), $KBrO_3$, KIO_4 and $(NH_4)_2S_2O_8$) on the degradation reaction was studied. Moreover, metal doping can improve the photocatalytic activity of MOF-5 due to the synergistic effect, narrow band gap and so on. The results show that Co/Zn-MOF-5 photocatalyst exhibited better photocatalytic activity than Ni/Zn-MOF-5 and raw MOF-5 for MB decolorization under UV and visible light irradiation. Furthermore, adding different electron acceptors, except TBHP, enhanced the photocatalytic performance of photocatalysts with a different rate. Also, kinetic studies revealed that the reactions follow pseudo-first-order. Additionally, bimetallic MOF-5s did not show obvious activity reduction in MB decolorization during five recycling usages.

***Keywords**: Bimetallic metal-organic frameworks, MOF-5, Photocatalyst, Methylene blue, Electron acceptor.*

1. Introduction

Organic pollutants such as various dyes releasing from textile, paper, leather, food and cosmetic industries, are one of the major serious worldwide problems. The removal of these organic pollutants has been an urgent and important issue because of their non-biodegradability, toxicity and unpleasant colouring as well as harmful effects on water [1]. Therefore, many researchers are trying to find ways to eliminate contaminants from wastewater [2,3].

Several physical and chemical decolorization techniques such as ion exchange, coagulation/flocculation treatment, biodegradation proceedings, oxidation methods, membrane filtration, adsorption onto activated carbon, sedimentation, steam stripping etc. have been utilized for the removal of dyes and other organic/inorganic pollutants. Current strategies have significant disadvantages such as incomplete ion removal, high-energy requirements, and production of toxic sludge or by-products requiring further disposal [4].

Among various methods, photocatalytic system is a well-known desirable solution to degrade environmental pollutants in wastewater [5]. In these processes, electron-hole pairs, which can react with water or oxygen molecules to produce OH or superoxide radicals, are generated upon irradiation of a semiconductor material, which displays a major role in degradation of pollutants. The electron transfer process is more efficient if the molecules are pre-adsorbed on the surface within a reasonable range and with an appropriate orientation [6–10]. It has been proven that supported semi- conductors are more effective than the unsupported one in photodegradation processes [11,12].

Metal-organic frameworks (MOFs) are organic-inorganic hybrid solids with immense and uniform crystalline coordination networks consisting of metal ions/clusters and organic linkers that connected together via coordination bonds. MOF-based materials have had

*Corresponding author.
E-mail address: a-fallah@guilan.ac.ir (A. Fallah Shojaei)

diverse applications in gas capturing and storage, chemical separation, catalysis, sensor devices, biomedicine and drug delivery, adsorption of organic molecules, luminescence, electrode materials, magnetism and carriers for nanomaterials [11]. Catalysis is of most promising applications of MOFs because of the benefits offered by the metal node centers (i.e. there is no leaching of metal ions and they have uniform centers) [12].

MOFs exhibit excellent photochemical activities as effective photocatalysts in homogeneous or heterogeneous processes [13]. These materials can be used as unique platforms for photo-induced removal of pollutants due to metal-containing nodes and organic linkers in MOFs. Furthermore, the band gap in MOFs systems is closely related to the HOMO–LUMO gap, allowing for fine-tuning and valid design of these photocatalysts at the molecular level [13]. In comparison with traditional semiconductor photocatalytic systems, photoactive MOF systems have superior properties including more efficiency in solar exploiting, tuneable active sites (i.e. metal-oxo clusters and organic linkers), high surface area, favourable porosity and photocatalytic system construction at the molecular level as well as fast transport and good compatibility for guest molecules [14]. For this purpose, MOFs would be ideal choices for light harvesting to achieve photocatalytic degradation of organic pollution.

The discovery of the first artificial photocatalytic system for pollutants degradation over mesoporous materials, zeolites, TiO_2, many metal oxides and sulfides including ZnO, Nb_2O_5, $MgFe_2O_4$, Bi_2O_3, CdS have been identified as active photocatalysts for photodegradation of organic pollutants in aqueous phase [3,7,15–20].

Furthermore, Garcia et al. reported that MOF-5 acts as a semiconductor upon light stimulation to emerge charge carriers (electrons and holes), which were capable to photocatalytically degrade phenol in aqueous solutions [21]. Zhang et al. reported Cu-doped ZIF-67 as a visible-light-driven photocatalyst for the degradation of methyl orange (MO) [22]. Chen et al. reported a twofold interpenetrated semiconducting MOF UTSA-38 represented photocatalytic activity for removal of MO from water solutions [23]. MOFs have also been used for the adsorptive removal of hazardous materials, such as desulfurization and denitrogenation processes [24–26]. Moreover, MOFs have been employed in the omission of several organics such as dyes [27,28], bisphenol-A [29,30], organic arsenic acids [31] and PPCPs (pharmaceuticals and personal care products) [32] from water. Obviously, MOFs have a bright future in photocatalysis in contaminant degradation.

In this work, the effect of metal centres of MOF-5s on photocatalytic decolorization of methylene blue dye were investigated. Also, the capability of raw MOF-5 and bimetallic MOF-5s (Co/Zn, Ni/Zn) were investigated to activate various electron acceptors such as H_2O_2, TBHP, $KBrO_3$, KIO_4 and $(NH_4)_2S_2O_8$ in order to achieve high efficiency under UV and visible photocatalytic processes. Furthermore, the effect of various operating parameters, such as catalyst loading, dye concentration and initial pH of dye solution were studied. Consequently, the adsorption kinetics were consistently explored according to Langmuir-Hinshelwood model.

2. Experimental

2.1. Materials

N,N-dimethylformamide (DMF), ethanol, dichloro-methane (CH_2Cl_2) and chloroform ($CHCl_3$) were purchased from Daejung (Korea), dried and distilled by standard techniques before using [33]. Zinc(II) nitrate hexahydrate, cobalt(II) nitrate hexahydrate, nickel(II) nitrate hexahydrate and 1,4-benzene dicarboxylic acid (terephthalic acid) were purchased from Merck. H_2O_2 (30% v/v), TBHP, $KBrO_3$, KIO_4 and $(NH_4)_2S_2O_8$ were purchased from Daejung. Methylene blue of AR grade was obtained from Merck.

2.2. Preparation of catalysts

Raw MOF-5 nanocrystals were synthesized with the same batch composition reported by He et al. [34] with some minor modifications. Briefly, the mixture of zinc(II) nitrate hexahydrate (297.5 mg, 1.0 mmol) and terephthalic acid (83 mg, 0.5 mmol) was dissolved in 7 ml DMF in a 10 ml vial. Then the mixture was transferred into a 25 ml Teflon-lined stainless-steel autoclave and heated in an oven at 100 °C for 24 hours. After cooling the reaction to room temperature, the solid product was filtered and washed with anhydrous DMF and CH_2Cl_2 (3×10 ml). Finally, it was dried in a vacuum oven at 60 °C for 4 h to afford pale yellow cubic crystals.

Modified Co/Zn-MOF-5 nanocrystals were synthesized by procedures reported by Botas et al. [35]. About 149 mg zinc(II) nitrate hexahydrate (0.5 mmol), 146 mg cobalt(II) nitrate hexahydrate (0.5 mmol) and 83 mg terephtalic acid (0.5 mmol) were dissolved in 24 ml DMF and 6 ml ethanol at room temperature. The mixture was transferred into a 43 ml Teflon-lined autoclave, which was sealed and maintained at 100 °C for 20 h. So, the reaction vessel was then removed from the oven and allowed to cool to room temperature. Produced solid was washed by anhydrous DMF and ethanol (3×10ml), then dried in a vacuum oven at 60 °C for 4 h. Consequently, purple crystals remained.

Modified Ni/Zn-MOF-5 nano/microcrystals were synthesized according to the previously reported procedure [36]. Totally, zinc(II) nitrate hexahydrate (446 mg, 1.50 mmol), nickel(II) nitrate hexahydrate (327 mg, 1.13 mmol), and terephthalic acid (83 mg, 0.50 mmol) were added into a 100 ml volume jar with a Teflon-lined autoclave. The contents were dissolved in 49 ml DMF and 1 ml deionized water. The solution was heated at 100 °C temperature for 7 h to afford pale green cubic crystals. The reaction container was cooled down at room temperature. The crystals were accumulated by centrifugation and washed with anhydrous DMF and CH_2Cl_2 (3× 10 mL). Finally, it was dried in the vacuum oven at 60 °C for 4 h, pale green crystals remained.

2.3. Instrumental and apparatus

SEM images were performed using a Philips, XL30 scanning electron microscope at 26 kV acceleration voltage. The XRD data were collected on a Philips PW1840 diffractometer with Cu-Kα radiation (1.5418C Å), the scan rate of 0.1° 2θ/s and within a range of 2θ of 2-50°. FT-IR spectra were recorded in the range of 400–4000 cm^{-1} on a Bruker Vector 22 FT-IR spectrophotometer utilizing KBr plates. The metal contents were analysed using inductively coupled plasma (ICP; Labtam 8440 plasma lab). Analysis of the metal-doped MOF-5s, after diluting with a low concentration of HNO_3, was used for the accurate determination of elements (Co and Ni). Elemental analysis was made by a Carlo-Erba EA1110 CNNO-S analyzer and agreed with the calculated values. Diffuse reflectance spectra were recorded with Perkin–Elmer Lambda 900 spectrophotometer in the range of 200-800 nm. UV-Vis spectra were obtained at room temperature on a UV-1800 RAILEGH spectrophotometer. For photocatalytic reactions, the irradiation was carried out under a high-pressure mercury lamp (HPMV 400W, Germany) as the UV light source and a 200 W xenon lamp as the visible light source. The lamp yields an illumination spectrum ranging from ultraviolet to visible range (200–800 nm).

2.4. Preparation of standard curve

First, an aqueous stock solution of MB (500 ppm) was prepared by dissolving 0.5 g of methylene blue in deionized water. Then different volumes of dye solution (1, 2, 4, 6, 8, 10, 12, 14, 16 and 18 ppm) were prepared from the stock solution to make a standard curve of absorbance vs. concentration. The wavelength in UV-Vis spectrophotometer was taken in the 200 - 800 nm range. The highest peak was achieved at 664 nm wavelength for MB dye. This wavelength was used during the entire experimental procedure. Standard curve was utilized to measure unknown concentration of MB.

2.5. Photocatalytic degradation of MB

The photocatalytic activities of bimetallic MOF-5s were evaluated by photodegradation of methylene blue dye in the electron acceptors attendance (H_2O_2, TBHP, $(NH_4)_2S_2O_8$, $KBrO_3$, KIO_4) in open air and at room temperature. To investigate photocatalytic degradation behavior of photocatalysts, the concentration of photocatalyst was assumed to be constant (0.25 g/L). To determine the adsorption capacity at various pHs, the pH of the MB solutions was adjusted with 0.1 M HCl or 0.1 M NaOH aqueous solution. Before irradiation, the suspension was magnetically stirred in dark environment for 60 min to ensure the establishment of an adsorption/desorption equilibrium, then a familiar concentration of electron acceptor (20 mM) was added to the solution mixture. During the photodegradation reaction, stirring was maintained to keep the mixture in suspension. The suspension was pulled out at predetermined time intervals and quickly centrifuged to get the supernatant for analysis. The concentration of MB was measured in λ_{max}= 664 nm in a 1 cm path length spectrometric quartz cell.

The percent of MB degradation was determined according to Eq. 1.

$$\text{MB degradation (\%)} = [(C_0\text{-}C)/C_0] \times 100 = [(A_0\text{-}A_t)/A_0] \times 100 \quad (\mathbf{1})$$

Where C_0 represents the initial concentration of the MB, C is the final concentration after irradiation, A_0 is the initial absorbance and A_t is the absorbance at various times.

3. Results and Discussion

3.1. Characterization of prepared catalysts

FT-IR spectra of synthesized MOF-5s are shown in Fig 1 (a). In the FT-IR spectra of the parent compound (Raw MOF-5) prominent bands at 1578 and 1381 cm^{-1} were attributed to the asymmetric and symmetric stretching of the carboxylate groups of the BDC linkers, respectively [37]. Several small bands in the region of 1146-1017 cm^{-1} and 820-600 cm^{-1} are attributed to the in-plane and out of plane stretching of the aromatic C-H groups of the benzene ring present in BDC linker, respectively. The bands around 3200-3500 cm^{-1} are related to the adsorbed moisture content [38]. The FT-IR spectra of metal doped samples (Co/Zn and Ni/Zn-MOF-5) are similar to their parent (Raw MOF-5), confirming the maintenance of the framework of raw MOF-5 during modification as expected from the literature [39].

As shown in Fig. 1 (b), XRD patterns confirmed that the structure of Co/Zn and Ni/Zn-MOF-5 were too far to become isostructural to raw MOF-5 by the overall patterns; it is similar to the results shown by Zhao et al. [40] and Hafizovic et al. [41]. A sharp peak below 10° (2θ = 9.4°) was observed in all samples, they indicate that MOF-5s are highly crystalline and suggesting that all of them did not change the morphology of crystal structure [41,42]. For Ni/Zn-MOF-5, the peak at 42.74° was the characteristic peak of metallic Ni with a face-centered cubic structure (JCPDS#87-0712). The peaks at 9.1°, 18.1°, 28.8°, 32.5°, 36.8°, 40.8°, 42.74° and 45.9° could be assigned to the diffraction peaks of parent MOF-5, this indicated that our raw MOF-5 support was well crystallized [43]. Also, the increasing trend in peaks intensity towards Ni/Zn-MOF-5 rather than other species indicates that better crystallinity towards the higher order; this is consistent with observations from the SEM images shown in Fig. 2 [40].

The pure phase of Co/Zn-MOF-5 nano crystals also suggests that the doped Co(II) ions should be well incorporated in the framework and substitutes for partial Zn(II) ions in the [Zn_4O] clusters, as observed in Ni-doped MOF-5 [43].

The average crystallite size was calculated using the XRD line broadening method by the following Scherrer's equation (Eq. 2) [44]:

$$d = \frac{k\lambda}{\beta \cos\theta} \qquad (2)$$

where d is the mean of crystallite diameter, k is the Scherrer constant (0.89), λ is the X-ray wavelength (nm), β is the full width at half maximum in radians, and θ is the Bragg angle of the 2 θ peak. The average sizes of the raw MOF-5, Co/Zn-MOF-5 and Ni/Zn-MOF-5 samples were estimated about 18.45, 29 and 29 nm respectively and are summarized in supplementary data, Table S1.

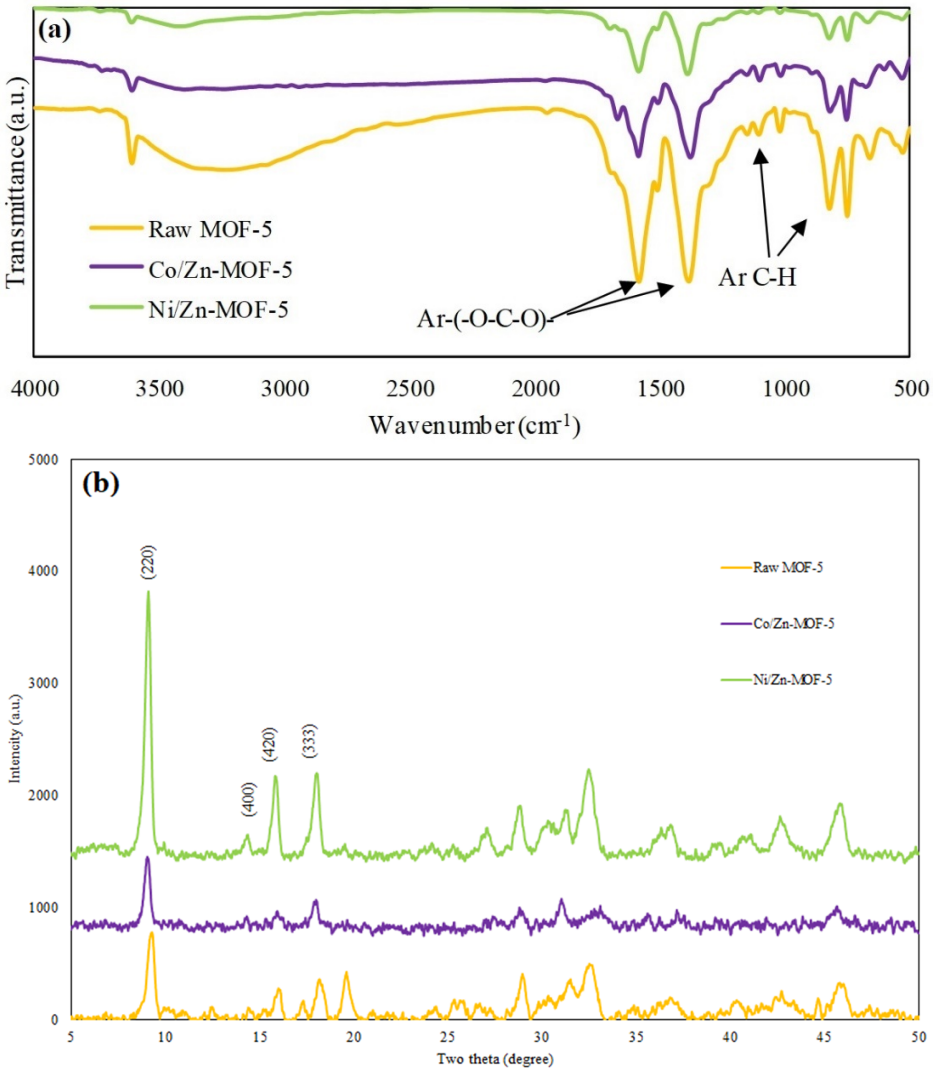

Fig. 1. FT-IR spectra (a) and XRD patterns (b) of as-prepared Co/Zn, Ni/Zn and raw MOF-5 samples

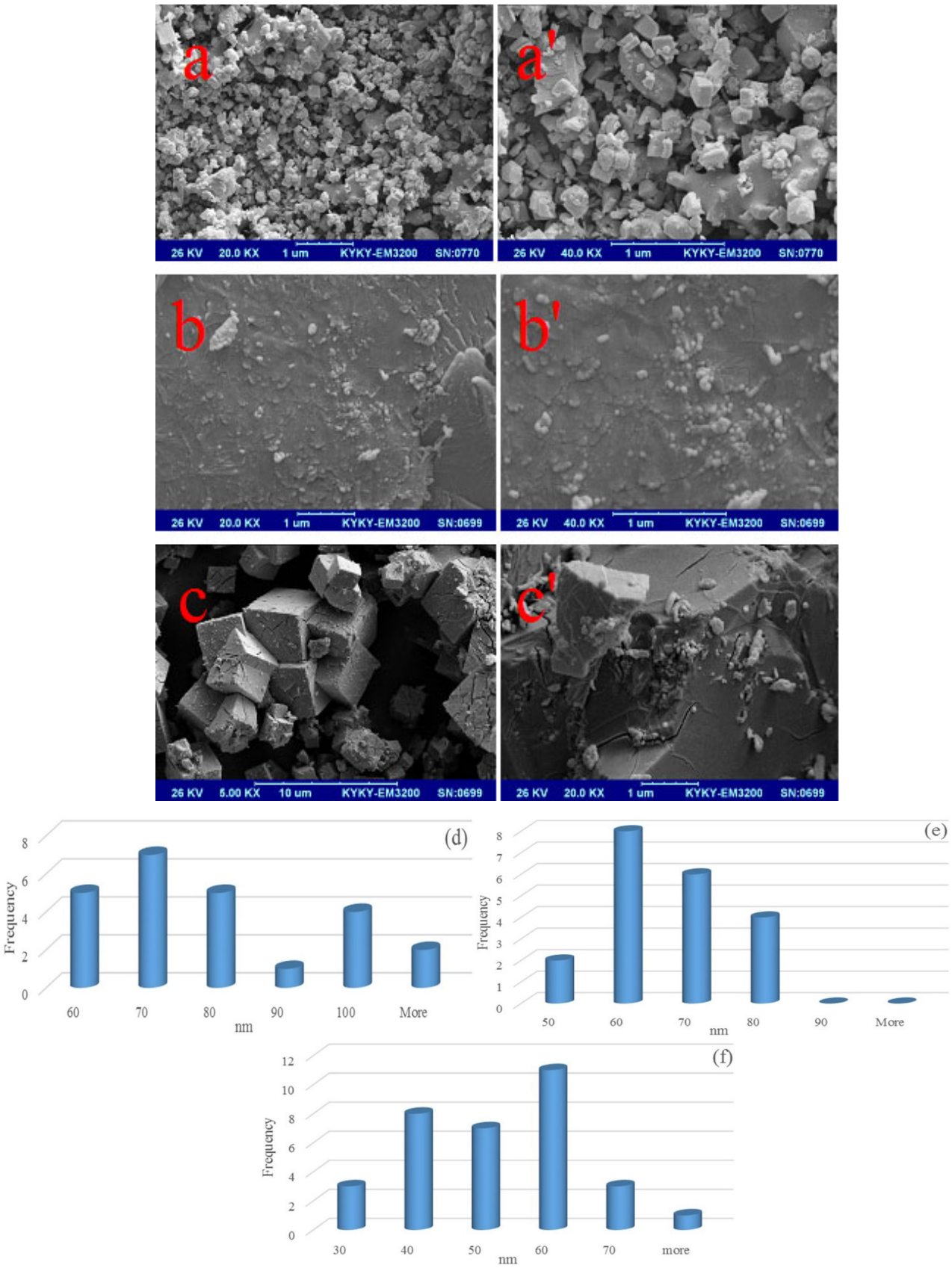

Fig. 2. SEM images of raw MOF-5 (a, a'), Co/Zn-MOF-5 (b, b'), Ni/Zn-MOF-5 (c, c'). Histogram distribution of raw MOF-5 (d), Co/Zn-MOF-5 (e) and Ni/Zn-MOF-5 (f).

The surface morphology and crystal size of the prepared samples as well as related histogram analyses, were determined by SEM images and are exhibited in Fig. 2 with different magnifications.

Raw MOF-5 morphology is characterized by cubic crystals with the approximate dimension of 70 nm in diameter (Fig. 2a, a'). Fig. 2b,b' show the SEM images of Co/Zn-MOF-5 nanoparticles. It demonstrates that entire particles are covered by interwoven rod-like structures with the average particle size of 60 nm. It is shown in Fig. 2c,c' that Ni/Zn-MOF-5 show very similar features with the particle size of 60 nm, suggesting that Ni-doping does not change the morphology of raw MOF-5. This result is consistent with the data reported in literature [45,46].

The optical properties of the prepared samples were investigated by diffuse reflectance spectroscopy (DRS). As can be seen in Fig. 3, raw MOF-5 displays a broad absorption peak at around 260 nm due to the $\pi(HOMO)\rightarrow\pi(LUMO)^*$ excitation of the terephthalic acid linkers [47]. The spectra of Co/Zn-MOF-5 display a broad peak around 550 nm, strongly revealing that the Co(II) is octahedrally coordinated [35]. The spectra of Ni/Zn- MOF-5 displaying bands at 420 and 720 nm, confirmed that the structure of Ni(II) complex was in an octahedral coordination [48]. The optical band gap may be determined by different procedures [49]. As a first approximation, the band gap energy (Eg) can be estimated directly by extrapolating the long wavelength edge of the peak in the absorbance spectrum to zero. More properly, it can be obtained by analyzing the dependence of the absorbance with the photon energy, according to the nature of the semiconductor (direct or indirect) [50]. The wavelength (λ) of absorbance edge of 320, 460 and 680 nm are reported for nanoparticles of raw MOF-5, Ni/Zn-MOF-5 and Co/Zn-MOF-5, respectively. Therefore, red shifts of 140 and 220 nm occurred in doped Ni(II) and Co(II) respectively. The band gap energies (E_g) of 3.87, 2.69 and 1.82 were calculated by the equation of E_g (eV) = 1239.84/λ (nm) for raw MOF-5, Ni/Zn-MOF-5 and Co/Zn-MOF-5 photocatalysts respectively.

Inductively Coupled Plasma (ICP) was used for more reliable measurement of metal contents of the synthesized materials. The ICP analysis indicates that the actual Co content of Co/Zn-MOF-5 is 35/65% and the actual Ni content of Ni/Zn-MOF-5 is 3.1%; these data agree well with the previously published crystal data [51].

Elemental analysis calculated for raw MOF-5: $Zn_4C_{24}H_{12}O_{13}$ (wt%): Zn 34.0, C 37.4, H 1.6, O 27.0, Found (wt%): Zn 33.8, C 37.7, H 1.7, O 26.8.

For Ni/Zn-MOF-5: $Zn_{3.63}Ni_{0.37}C_{24}H_{12}O_{13}$ with a yield of 68% based on BDC, containing 3.1% Ni and 96.89 % Zn. Calculated (%): C 37.65, H 1.52, N 0.00; Found (%): C: 37.40, H 1.80, N 0.00.

For Co/Zn-MOF-5: $Zn_{0.36}Co_{3.64}C_{24}H_{12}O_{13}$ with a yield of 80% based on BDC, comprising 35.65% Co and 64.35% Zn. Calculated (%): C 36.90, H 2.48, N 0.00; Found(%): C 37.30, H 2.90, N 0.00.

3.2. Photocatalytic activities

The degradation of MB under UV and visible light sources was investigated in the presence of bimetallic MOF-5s (Fig. 4). The result revealed that Ni/Zn-MOF-5 showed the highest adsorption property (9.73%) among other catalysts in dark. Therefore, the adsorption of dye on the catalyst is very small and the occurring process is photocatalysis.

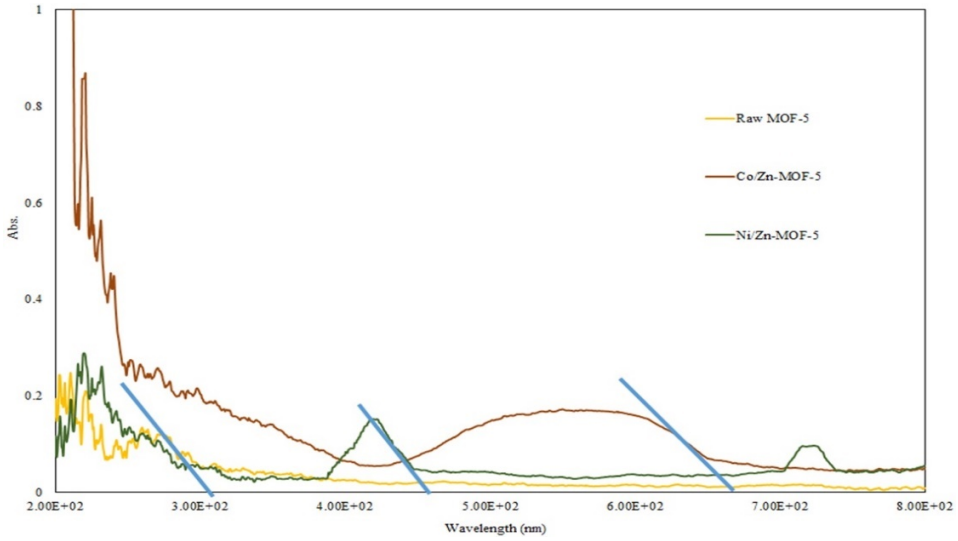

Fig. 3. DRS spectra of as-prepared Co/Zn, Ni/Zn and raw MOF-5 samples.

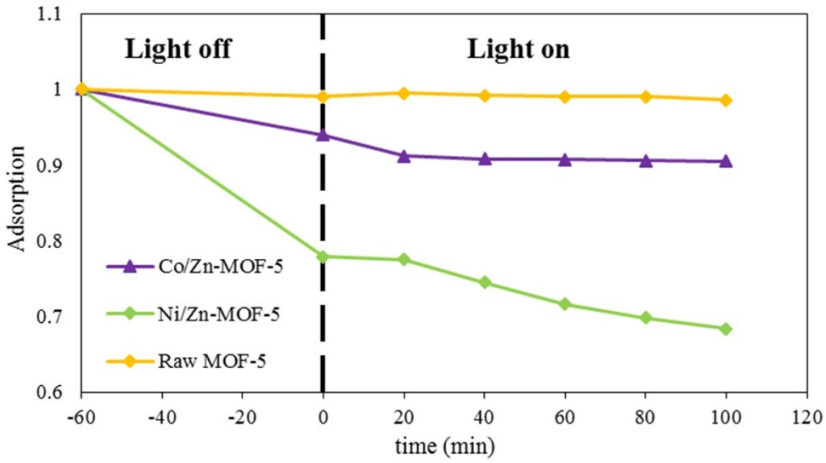

Fig. 4. Photocatalytic degradation of MB by bimetallic Co/Zn, Ni/Zn and raw MOF-5 under UV light irradiation (the initial concentration of dye = 12 mg/L, dosage of catalyst = 0.25 g/L, pH 4, time = 100 min, room temperature).

The reaction mechanism for MB decolorization could be discussed based on the semiconductor theory [52]. Ultraviolet or visible light incident on bimetallic MOF-5s photocatalysts can excite an electron from the valence band to the conduction band, this generates holes in the valence band. These photoexcited electrons can reduce molecular oxygen to superoxide radical, which have strong oxidation capability for decolorization of MB molecules. Consequently, the photogenerated holes with strong oxidation ability can oxidize hydroxyl ions or water molecules to afford hydroxyl radical. Reactive oxygen species can damage molecules and cell structures and processes which enable applications such as self-cleaning surfaces, disinfection, degradation and oxidation of contaminants [52].

As shown in Fig. 4, the photodegradation utility of MB is very low over the raw MOF-5 photocatalyst (2%), without electron acceptors. It could be ascribed to the fast electron–hole recombination. When electron acceptors and photocatalysts were added into the solution simultaneously, the photocatalytic utility was noticeably improved because the electron acceptor would prevent the electron–hole pair recombination, thus it enhances the photodegradation utility [53].

Due to MB absorption molecules on photocatalysts' surfaces and electrons' quick decay from excited state to the ground state, the photocatalytic degradation of MB dye by photocatalysts is low. Photons reduction, which are absorbed by photocatalysts, may cause the decreased MB photodegradation rate. Consequently, adding the electron acceptor enhances the performance of the photocatalysts due to producing radicals [51].

Adding hydrogen peroxide (H_2O_2), potassium bromate ($KBrO_3$), potassium iodate (KIO_4) and ammonium persulfate [$(NH_4)_2S_2O_8$], as electron acceptors can prevent the electron–hole pair recombination according to Eqs. (3)–(6). Therefore, these electron acceptors enhance the photodegradation efficiency via generating more radicals ($^{\bullet}OH$, $BrO_2^{\bullet}$, $IO_3^{\bullet}$ and $SO_4^{\bullet-}$).

$$H_2O_2 + e^- \rightarrow OH^{\bullet} + OH^- \quad (3)$$

$$BrO_3^- + 2H^+ + e^- \rightarrow BrO_2^{\bullet} + H_2O \quad (4)$$

$$S_2O_8^{2-} + e^- \rightarrow SO_4^{2-} + SO_4^{-\bullet} \quad (5)$$

$$IO_4^- + 2H^+ + e^- \rightarrow IO_3^{\bullet} + H_2O \quad (6)$$

e Effect electron acceptor adding on bimetallic MOF-5s photocatalysts efficiency was studied photocatalytically. Fig. 5 demonstrates the time period (100 min) of MB photodegradation in presence of different electron acceptors over bimetallic MOF-5s photocatalysts. The concentration of electron acceptors in all experiments were constant (20 mM). As shown in Fig. 5, adding different electron acceptors, except TBHP, enhance the photocatalytic performance of photocatalysts under UV and visible light irradiation. The enhanced rate follows the order of H_2O_2 > $(NH4)_2S_2O_8$ > KIO_4> $KBrO_3$> TBHP for Co/Zn-MOF-5 [see Fig. 5 (a), (b)]. Also, it is in the order of $(NH_4)_2S_2O_8$ > KIO_4> H_2O_2 > $KBrO_3$> TBHP under UV and visible light irradiation for Ni/Zn-MOF-5 and raw MOF-5 [see Fig. 5 (c)-(f)].

Adding H_2O_2 solution (20 mM) to the reaction vessel enhances the rate of MB decolorization. For Co/Zn-MOF-5 about 98% degradation of MB was observed after 100 min of UV light irradiation, while with the use of $(NH_4)_2S_2O_8$ as electron acceptor species, for Ni/Zn-MOF-5 and raw MOF-5 about 91% and 72.1% degradation of MB were observed under UV light irradiation, respectively.

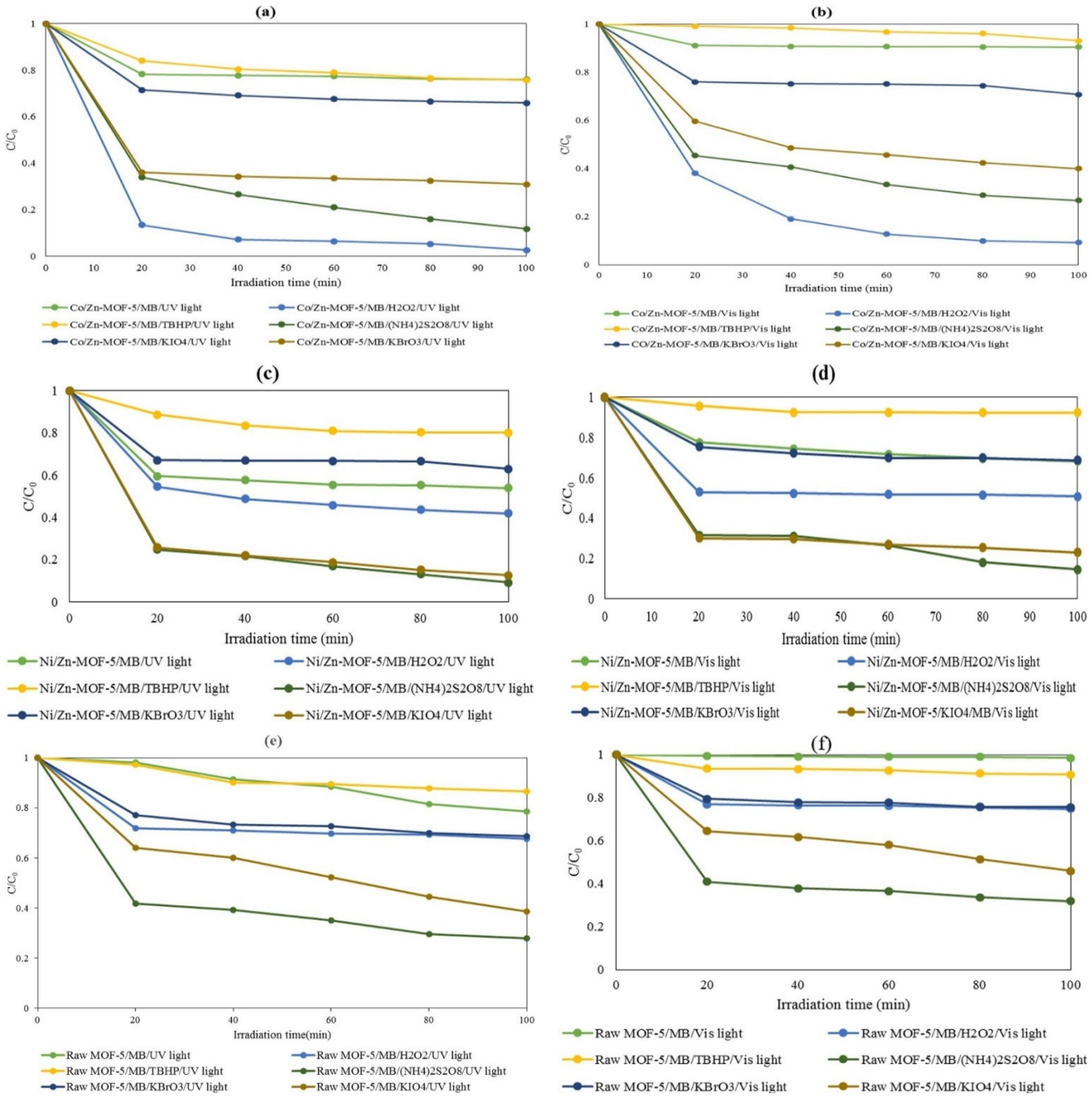

Fig. 5. The effect of different electron acceptor additives on the MB photodegradation in the presence of Co/Zn-MOF-5 under UV (a), Co/ZnMOF-5 under visible light (b), Ni/Zn-MOF-5 under UV (C), Ni/Zn-MOF-5 visible light (d), raw MOF-5 under UV (e), raw MOF-5 under visible light irradiation (f). In the presence of $(NH_4)_2S_2O_8$ (full squares), KIO_4 (open squares), H_2O_2 (full circles), $KBrO_3$ (open circles), TBHP (full triangles) and without oxidant (open triangles). (The initial concentration of dye = 12 mg/L, dosage of catalyst= 0.25 g/L, dosage of electron acceptor = 20 mM, pH 4, time = 100 min, room temperature).

Compared to hydroxyl radicals with a standard redox potential of 1.8–2.7 V, sulfate radicals with standard redox potential of 2.5–3.1 V is more selective for oxidation. Furthermore, persulfate has a low energy input, and it is a cost-effective and environmentally friendly oxidant [54].

The high degradation rate in the presence of H_2O_2 (for Co/Zn-MOF-5) and $(NH_4)_2S_2O_8$ (for Ni/Zn- and raw MOF-5) than $KBrO_3$, TBHP and KIO_4, is due to the suitable electron trapping, thereby preventing the recombination of photoexcited electrons, photogenerated holes, thus it increases the number of hydroxyl and sulfate radicals.

All electron acceptors increase the speed of reaction except TBHP. TBHP behavior's explanation is a chain reaction which is terminated by undesirable reactions where radicals are consumed before creating new radicals. Consequently, the destruction reaction speed is even less than when electron acceptors are not used. Surprisingly, this phenomenon is not reported yet.

Previous studies reported that the metal centers of MOFs show nil effect on the photocatalytic activity for MB photodegradation [52]. Co/Zn- and Ni/Zn-MOF-5 are isostructural to raw MOF-5. Therefore, a study on isostructural photocatalysts can provide valuable information about the effect of metal centres of isoreticular MOFs photocatalysts on their photocatalytic activities. Therefore, it can be anticipated that Co/Zn-MOF-5 has the highest rate for MB degradation since it has a narrow band gap (1.82 eV) in comparison with Ni/Zn- and raw MOF-5. Co/Zn-MOF-5 enhances the utilization efficiency of solar energy and also promote the separation of photogenerated holes and photoexcited electrons sufficiently due to narrowing the band gap which caused high photodegradation of MB under UV and visible light irradiation. To clarify the present condition, more experimental and computational studies are needed.

3.3. Effect of the solution pH

The solution pH is an important factor that could remarkably affect the catalytic reaction. The effect of initial pH on the degradation efficiency of MB over bimetallic MOF-5s/light/electron acceptor system was determined. As shown in Fig. 6 (a), the catalysts could work effectively over a wide pH range from 2.0 to 10.0. It is believed that diversity in the surface charge properties of a photocatalyst and the charge of the dye molecules account for pH depend on the photocatalyst process [55]. pH variation may affect dye molecules adsorption into catalyst's surface, this is perceived as a substantial step for photocatalytic oxidation. The OH radical can be engendered by the reaction between hydroxide ion and positive hole as well. An alkaline circumstance enhances OH radical formation then it strengthens degradation efficiency. The most rapid MB decolorization happens when pH measure is 4. In other words, the formation of OH radical by hydroxyl ions' oxidation with photogenerated holes becomes desirable when pH is 4. Additionally, the zero-point charge for MOF-5 was acquired around 7.2 [56]. The catalyst surface charge is positive when pH values are smaller than the pH_{pzc} [57]. Otherwise, it is negative. MB adsorption is desirable when pH values are higher than the pH_{pzc} thanks to its cationic configurations [50].

Predictably, the photocatalytic efficiency must be empowered in most alkaline pH in which hydroxyl radical is derived. Although, results acquired by alkaline pH are as the same as our expectancy. It may be described as follows: H_2O_2 and $HO_2^{\bullet}$ radicals can be formed owing to the reaction of OH radical with ^{-}OH in ^{-}OH high concentration. Therefore, the radical–radical reactions also occurs which results in the hydroxyl radicals are deactivated due to high amounts of OH radicals presence [53]. Dye adsorption in this pH may cause a significant loss in MB at the initial contact time of the process in alkaline pH. As shown in Fig. 6 (a), the catalyst demonstrates better adsorption feature resulting in better photocatalytic activity when pH value is equal to 4 [58]. This may be caused by the fact that oxidizing factors are not stable in the alkaline medium and tend to decompose to their constituent molecules.

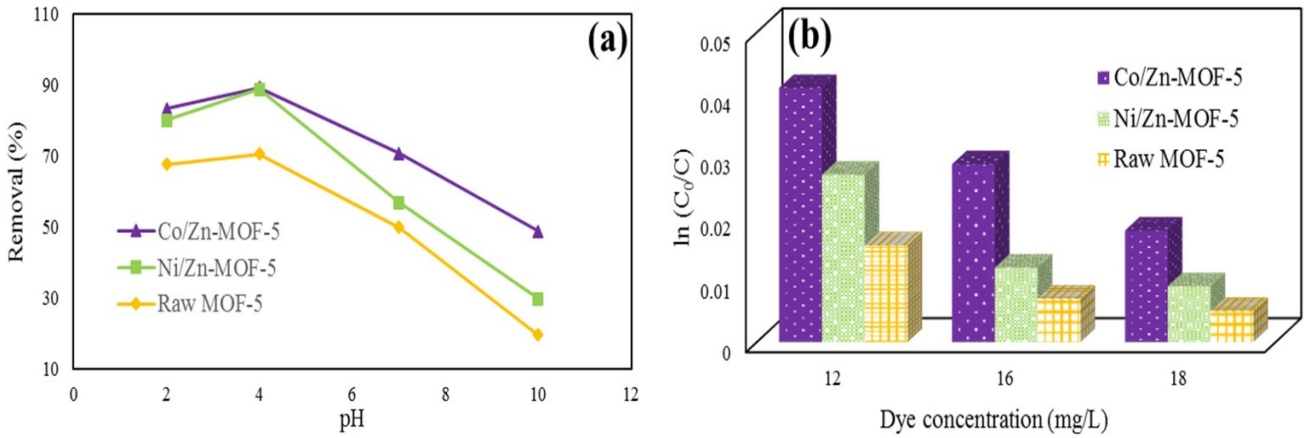

Fig. 6. Effect of initial solution pH (the initial concentration of dye = 12 mg/L, dosage of catalyst = 0.25 g/L, time = 100 min) (a) and effect of initial dye concentration on dye removal (pH 4, dosage of catalyst = 0.25 g/L, time = 100 min, room temperature).

3.4. Effect of catalyst loading

Catalyst loading is one of the significant parameters in a photocatalytic process. Therefore, experiments were carried out to assess an optimum amount of catalyst dosage for the reaction. Effects of raw MOF-5 and bimetallic MOF-5s concentrations on the photodegradation of MB dye by varying amount of catalysts from 0.25-0.45 g/L at constant dye concentration = 12 mg/L, electron acceptor = 20 mM and pH 4.0 were investigated during 100 min irradiation time. Therefore, the catalyst dosage was set to 0.25 g/l for future researches. The dosage effects on the degradation process was examined as well. As shown in Table 1, the degradation activity rose first, then fell when the catalyst mass raised from 0.15 g/l to 0.25 g/l. The most substantial parameters which resulted in light absorption reduction by photocatalyst particles, are light scattering, screening effects as well as agglomeration tendency (particle-particle interaction) [59]. Subsequently, there are fewer semiconductor particles which can excite. Moreover, the degradation rate of the pollutant tends to decrease at a high dosage of catalyst because of engendering less electron/holes and hydroxyl radicals. The desired point seems to be that when light cannot penetrate due to the intense particle concentration nonetheless the amount of active sites in solution will ascend by rising catalyst loading. These two paradox phenomenon interaction cause an optimal catalyst loading for photocatalytic reactions [60].

3.5. Effect of dye concentration

The initial MB concentration has a substantial effect on the rate of photodegradation and this was determined for all the catalysts by varying the dye concentration from 12-18 mg/L and by maintaining the other parameters constant (catalyst loading of 0.25 g/L, pH 4, electron acceptor = 20 mM). As shown in Fig. 6 (b), the decolorization was at its highest point in 12 mg/l MB solution. Hydroxyl radicals just can react where they formed due to minuscule lifespan that they have. Rising MB molecules per volume unit strengthen the collision possibility between hydroxyl radicals which increase decolorization efficiency [61]. Reportedly, degradation efficiency of dye decreased when the primary concentration increased to more than 12 mg/L. By increasing the amount of dye, more dye molecules are absorbed on the photocatalyst surface. Consequently, the catalyst active sites reduce. Furthermore, increasing dye concentration causes a reduction in photons numbers reaching the catalyst surface. Indeed, more photons were absorbed by dye molecules and photocatalyst particles excitement by photons was reduced based on the literature [62]. The formed intermediates (including organic acids, ketones, aldehydes and aromatics) during the dye photodegradation were interacted with dye molecules for limited adsorption on sites on the catalyst surface and avoided MB decolorization [63].

3.6. Kinetic study

The photodegradation of MB dye follows the pseudo-first order kinetics according to the Langmuir-Hinshelwood model, so the photodegradation rate of MB dye was studied by the following equation (Eq. 7) [7,64]:

$$ln\frac{C}{C_0} = -kt \qquad (7)$$

Where C_0 is the initial concentration of dye at t = 0 min, C is the concentration of dye at irradiation time 't' and k is the apparent rate constant. The curves of variation in $\ln(C_0/C)$ vs. irradiation time are given in Fig. 7. The slope of the Ln C_0/C_t vs. plot gives the value of the rate constant k in min^{-1}. The k values, which are obtained by linear fitting from Table 2 are 0.0176, 0.0125 and .0054 min^{-1} for Co/Zn-MOF-5, Ni/Zn-MOF-5 and raw MOF-5, respectively. It can be seen from Table 2 that the k value of Co/Zn-MOF-5 is 0.0176 min^{-1}, which is higher than the other photocatalysts.

3.7. Stability of catalysts

The reusability of a heterogeneous catalysts is of prime emphasis not only from the economic standpoint but also because of the easy work-up procedure. The homogeneous catalysts cannot be recovered even once, although the heterogeneous catalysts can be easily filtered and reused multiple times without noticeable loss of catalytic activity.

Table 1. Variation of the rate constant with catalysts loading in the presence of catalysts.

Catalysts	k values (min^{-1})			
	0.15 g/L	0.25 g/L	0.35 g/L	0.45 g/L
Co/Zn-MOF-5	0.0153	0.0176	0.013	0.007
Ni/Zn-MOF-5	0.009	0.0125	0.0058	0.0032
Raw MOF-5	0.0028	0.0054	0.0007	0.0004

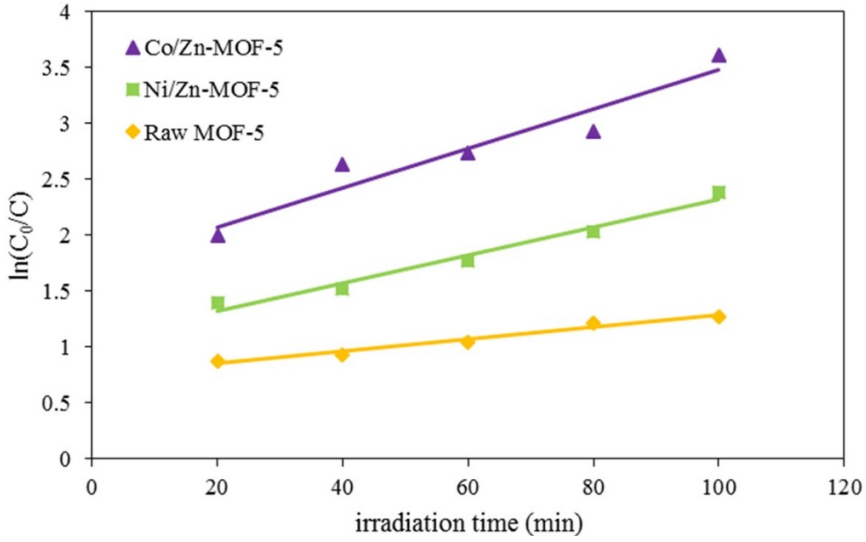

Fig. 7. Kinetics of the photocatalytic degradation of MB by bimetallic Co/Zn, Ni/Zn and raw MOF-5 under UV light irradiation (the initial concentration of dye = 12 mg/L, dosage of catalyst = 0.25 g/L, pH 4, time = 100 min, room temperature).

Table 2. Pseudo-first-order kinetics for the photocatalytic degradation of MB dye by different catalysts.

Sample	Fitted equation	Reaction rate constant, k (min^{-1})	Correlation coefficient, R
Co/Zn-MOF-5	y=0.0176x+1.726	0.0176	0.922
Ni/Zn-MOF-5	y=0.125x+1.0741	0.0125	0.9758
Raw MOF-5	y=0.0054x+0.7446	0.0054	0.9747

The stability of catalysts was monitored using the multiple sequential photocatalytic degradation reaction. For every repeated reaction, the catalyst was filtered, washed with distilled hot water and ethanol, dried in a vacuum oven (60 °C for 4 h) before being used. The catalysts were consecutively reused five times without detectable loss of their activities, indicating that bimetallic MOF-5s has excellent long-term stability (Fig. 8).

3.8. Adsorption mechanism

Even though a more detailed study is necessary to clarify the mechanism of MB adsorption/degradation on bimetallic MOF-5s, the adsorption may be explained by an electrostatic interaction between the dye and adsorbent[52]. MB exists in positive form, therefore there will be an electrostatic interaction with an adsorbent having a negative charge. As explained above, when the pH increases from 2 to 4, the amount of MB degraded when Co/Zn-MOF-5 increases from 83.41 to 90 %; this displays the electrostatic interaction role in degradation process. Possibly, Co^{2+} is more effective than Ni^{2+} and Zn^{2+} because of its smaller size, narrow band gap etc. However, another mechanism like π-π interaction[38] between benzene rings of bimetallic MOF-5s and MB cannot be ruled out. Preliminary experiments indicate that Co/Zn-MOF-5 may have a potential application in the removal of MB.

4. Conclusions

Bimetallic MOF-5s (Co/Zn and Ni/Zn) were synthesized via a simple solvothermal method. Samples were characterized with FT-IR, XRD, SEM, DRS, ICP and EA techniques. Photocatalytic activities of photocatalysts were investigated in dark, UV and visible light irradiation. Also, the effects of adding electron acceptor, solution pH, catalyst loading and dye concentration were evaluated. The results showed that photocalytic activity of Co/Zn-MOF-5 is better than Ni/Zn and raw MOF-5, due to the difference in the band gap, its smaller size and the synergistic effect. Adding different electron acceptors enhances the photocatalytic performance of photocatalysts, except TBHP. Optimum reaction conditions (such as dye concentration, dosage of catalyst, pH) were determined and an investigation of kinetics revealed that the reactions follow pseudo-first-order. Moreover, bimetallic MOF-5s used in this study did not exhibit any obvious loss of activities for MB decolorization during five repeated usages.

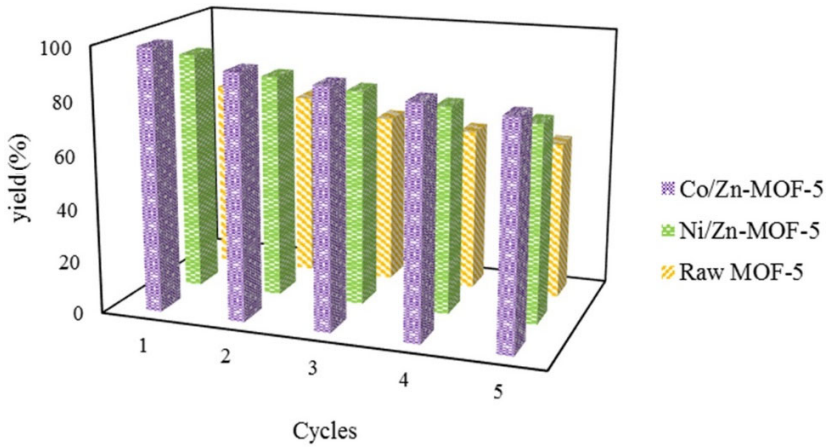

Fig. 8. Photodegradation efficiency of MB over bimetallic Co/Zn, Ni/Zn and raw MOF-5 photocatalysts after five repetitive use (the initial concentration of dye = 12 mg/L, dosage of catalyst = 0.25 g/L for each cycle, pH 4, time = 100 min, room temperature).

Acknowledgements

The financial support of this work by University of Guilan research council is gratefully acknowledged.

References

[1] S.K. Ling, S. Wang, Y. Peng, J. Hazard. Mater. 178 (2010) 385–389.
[2] M.N. Chong, B. Jin, C.W.K. Chow, C. Saint, Water Res. 44 (2010) 2997–3027.
[3] A. Buthiyappan, A.R. Abdul Aziz, W.M.A. Wan Daud, Rev. Chem. Eng. 32 (2016) 1–47.
[4] A. Nezamzadeh-Ejhieh, M. Khorsandi, J. Hazard. Mater. 176 (2010) 629–637.
[5] S. Subudhi, D. Rath, K.M. Parida, Catal. Sci. Tech. (2018).
[6] H. Derikvandi, A. Nezamzadeh-Ejhieh, J. Mol. Catal. A: Chem. 426 (2016) 158-169.
[7] H. Zabihi-Mobarakeh, A. Nezamzadeh-Ejhieh, J. Ind. Eng. Chem. 26 (2015) 315-321.
[8] S. Dianat, Iran. J. Catal. 8 (2018) 121–132.
[9] P. Dhiman, M. Naushad, K.M. Batoo, A. Kumar, G. Sharma, A.A. Ghfar, G. Kumar, M. Singh, J. Cleaner Prod. 165 (2017) 1542-1556.
[10] M. Pirhashemi, A. Habibi-Yangjeh, J. Photochem. Photobiol. 363 (2018) 31–43.
[11] M.H. Yap, K.L. Fow, G.Z. Chen, Green Energy Environ. 2 (2017) 218–245.
[12] Z. Sun, G. Li, Y. Zhang, H.O. Liu, X. Gao, Catal. Commun. 59 (2015) 92–96.
[13] J. Long, S. Wang, Z. Ding, S. Wang, Y. Zhou, L. Huang, X. Wang, Chem. Commun. 48 (2012) 11656–11658.
[14] C.G. Silva, A. Corma, H. García, J. Mater. Chem. 20 (2010) 3141-3156.
[15] H.R. Pouretedal, M. Ahmadi, Iran. J. Catal. 3 (2013) 149–155.
[16] A.B. Ghomi, V. Ashayeri, Iran. J. Catal. 2 (2012) 135–140.
[17] A. Nezamzadeh-Ejhieh, M. Khorsandi, Iran. J. Catal. 1 (2011) 99–104.
[18] M.H. Habibi, E. Askari, Iran. J. Catal. 1 (2011) 41–44.
[19] S.A. Hosseini, R. Saeedi, Iran. J. Catal. 7 (2017) 37–46.
[20] N.E. Fard, R. Fazaeli, Iran. J. Catal. 8 (2018) 133–141.
[21] M. Alvaro, E. Carbonell, B. Ferrer, F.X. Llabrés I Xamena, H. Garcia, Chem. Eur. J. 13 (2007) 5106–5112.
[22] H. Yang, X.-W. He, F. Wang, Y. Kang, J. Zhang, J. Mater. Chem. 22 (2012) 21849–21851.
[23] M.C. Das, H. Xu, Z. Wang, G. Srinivas, W. Zhou, Y.-F. Yue, V.N. Nesterov, G. Qian, B. Chen, Chem. Commun. 47 (2011) 11715-11717.
[24] I. Ahmed, Z. Hasan, N.A. Khan, S.H. Jhung, Appl. Catal. B 129 (2013) 123–129.
[25] I. Ahmed, N.A. Khan, Z. Hasan, S.H. Jhung, J. Hazard. Mater. 250–251 (2013) 37–44.
[26] I. Ahmed, N.A. Khan, S.H. Jhung, Inorg. Chem. 52 (2013) 14155–14161.
[27] S.-H. Huo, X.-P. Yan, J. Mater. Chem. 22 (2012) 7449–7455.
[28] M.M. Tong, D.H. Liu, Q.Y. Yang, S. Devautour-Vinot, G. Maurin, C.L. Zhong, J. Mater. Chem. A 1 (2013) 8534–8537.
[29] E.Y. Park, Z. Hasan, N.A. Khan, S.H. Jhung, J. Nanosci. Nanotechnol. 13 (2013) 2789–2794.
[30] M. Zhou, Y. nan Wu, J. Qiao, J. Zhang, A. McDonald, G. Li, F. Li, J. Colloid Interface Sci. 405 (2013) 157–163.
[31] J.W. Jun, M. Tong, B.K. Jung, Z. Hasan, C. Zhong, S.H. Jhung, Chem. Eur. J. 21 (2015) 347–354.
[32] Z. Hasan, E.-J. Choi, S.H. Jhung, Chem. Eng. J. 219 (2013) 537–544.
[33] T. Welton, Chem. Rev. 99 (1999) 2071–2083.
[34] Y. He, B. Li, M. O'Keeffe, B. Chen, Chem. Soc. Rev. 43 (2014) 5618–5656.
[35] J.A. Botas, G. Calleja, M. Sánchez-Sánchez, M.G. Orcajo, Langmuir 26 (2010) 5300–5303.
[36] C.K. Brozek, M. Dincă, Chem. Sci. 3 (2012) 2110-2113.
[37] R. Sabouni, H. Kazemian, S. Rohani, Chem. Eng. J. 165 (2010) 966–973.

[38] S.M. Sabet, H. Mahfuz, A.C. Terentis, J. Hashemi, B. Boesl, Mater. Lett. 168 (2016) 9–12.
[39] J.M. Yang, Q. Liu, W.Y. Sun, J. Solid State Chem. 218 (2014) 50–55.
[40] L.Y.S. Zhao Z. Li Z, Ind. Eng. Chem. Res. 48 (2009) 10015–10020.
[41] J. Hafizovic, M. Bjørgen, U. Olsbye, P.D.C. Dietzel, S. Bordiga, C. Prestipino, C. Lamberti, K.P. Lillerud, J. Am. Chem. Soc. 129 (2007) 3612–3620.
[42] D. Saha, S. Deng, Z. Yang, J. Porous Mater. 16 (2009) 141–149.
[43] H. Li, W. Shi, K. Zhao, H. Li, Y. Bing, P. Cheng, Inorg. Chem. 51 (2012) 9200–9207.
[44] A. Nezamzadeh-Ejhieh, S. Tavakoli-ghinani, C.R. Chim. 17 (2014) 49-61.
[45] J.-R. Li, R.J. Kuppler, H.-C. Zhou, Chem. Soc. Rev. 38 (2009) 1477–1504.
[46] N. Stock, S. Biswas, Chem. Rev. 112 (2012) 933–969.
[47] L. Zhang, Y.H. Hu, Phys. Lett. A 375 (2011) 1514–1517.
[48] G.R. Desiraju, J. Am. Chem. Soc. 135 (2013) 9952–9967.
[49] M. Nowak, B. Kauch, P. Szperlich, Rev. Sci. Instrum. 80 (2009) 4–7.
[50] P. Wurfel, Physics of solar cells from principles to new concepts, First ed., Wiley-VCH, Weinheim, 2005.
[51] K.K. Tanabe, S.M. Cohen, Chem. Soc. Rev. 40 (2011) 498–519.
[52] J.J. Du, Y.P. Yuan, J.X. Sun, F.M. Peng, X. Jiang, L.G. Qiu, A.J. Xie, Y.H. Shen, J.F. Zhu, J. Hazard. Mater. 190 (2011) 945–951.
[53] A. Eslami, A. Oghazyan, M. Sarafraz, Iran. J. Catal. 8 (2018) 95–102.
[54] X. Li, W. Guo, Z. Liu, R. Wang, H. Liu, Appl. Surf. Sci. 369 (2016) 130–136.
[55] S.E.H. Etaiw, M.M. El-bendary, Appl. Catal. B 126 (2012) 326–333.
[56] N. Bakhtiari, S. Azizian, J. Mol. Liq. 206 (2015) 114–118.
[57] A. Nezamzadeh-Ejhieh, M. Karimi-Shamsabadi, Chem. Eng. J. 228 (2013) 631–641.
[58] S. Zhang, X. Zhao, H. Niu, Y. Shi, Y. Cai, G. Jiang, J. Hazard. Mater. 167 (2009) 560–566.
[59] L. Ai, C. Zhang, L. Li, J. Jiang, Appl. Catal. B 148–149 (2014) 191–200.
[60] N. Ajoudanian, A. Nezamzadeh-Ejhieh, Mater. Sci. Semicond. Process. 36 (2015) 162–169.
[61] M. Hossein, N. Talebian, J. Choi, Dyes Pigm. 73 (2007) 103–110.
[62] A. Nezamzadeh-Ejhieh, H. Zabihi-Mobarakeh, J. Ind. Eng. Chem. (2013) 1–11.
[63] Z. Shams-ghahfarokhi, A. Nezamzadeh-Ejhieh, Mater. Sci. Semicond. Process. 39 (2015) 265–275.
[64] S.D. Khairnar, M.R. Patil, V.S. Shrivastava, Iran. J. Catal. 8 (2018) 143–150.